Food Chemistry 282 (2019) 18–26

Contents lists available at ScienceDirect

Food Chemistry

journal homepage: www.elsevier.com/locate/foodchem

Tyrosinase based amperometric biosensor for determination of tyramine in fermented food and beverages with gold nanoparticle doped poly(8-anilino-1-naphthalene sulphonic acid) modified electrode

Wanderson da Silva[a], Mariana Emilia Ghica[a], Rachel F. Ajayi[b], Emmanuel I. Iwuoha[b], Christopher M.A. Brett[a,*]

[a] Department of Chemistry, Faculty of Sciences and Technology, University of Coimbra, 3004-535 Coimbra, Portugal
[b] SensorLab, Department of Chemistry, University of Western Cape, 7535 Bellville, Cape Town, South Africa

ARTICLE INFO

Keywords:
Tyramine
Tyrosinase
Nanocomposite
Gold nanoparticles
Poly-(8-anilino-1-naphthalene sulphonic acid)
Food monitoring

ABSTRACT

The aim of the present work was to develop an amperometric biosensor for tyramine (Tyr) measurement in food and beverages. The biosensor architecture is based on tyrosinase (Tyr_{ase}) immobilization on glassy carbon electrode modified by a nanocomposite consisting of gold nanoparticles (AuNP) synthesized by a green method and poly(8-anilino-1-naphthalene sulphonic acid) modified glassy carbon electrode. Under optimized experimental conditions for fixed potential amperometric detection, the biosensor exhibited a linear response to tyramine in the range 10–120 μM and the limit of detection was estimated to be 0.71 μM. The novel platform showed good selectivity, long-term stability, and reproducibility. The strong interaction between tyrosinase and the nanocomposite was revealed by the high value of the Michaelis-Menten constant (79.3 μM). The fabricated biosensor was successfully applied to the determination of Tyr in dairy products and fermented drinks with good recoveries, which makes it a promising biosensor for quantification of tyramine.

1. Introduction

Tyramine (4-hydroxyphenethylamine, Tyr), is one of the well-known biogenic amines produced by decarboxylation of the amino acid tyrosine, due to microbial activity. It is commonly found in fermented foods and beverages, such as meat, seafood, dairy products, wine and beer. Tyr indirectly acts as a sympathomimetic amine which releases norepinephrine from sympathetic amine nerve endings, and it has been reported that Tyr-containing foods can cause serious intoxication effects when ingested in large quantities by eating contaminated foods (Atta & Abdel-Mageed, 2009; Galgano, Favati, Bonadio, Lorusso, & Romano, 2009). Consequently, the control and measurement of biogenic amines, mainly Tyr, is gaining importance in monitoring production processes and quality and freshness for food safety.

Analytical methods used for the quantification and determination of this kind of compounds include high-performance liquid chromatography (HPLC), ultra-performance liquid chromatography (UPLC), gas chromatography (GC), thin-layer chromatography (TLC), ion-pair liquid chromatography (IPLC), and capillary electrophoresis (CE), as in (Bacaloni, Insogna, Sancini, Ciarrocca, & Sinibaldi, 2013; Cheng, Zhang, Wang, Huang, & Ma, 2017; Cinquina et al., 2004; Ordóñez, Troncoso, García-Parrilla, & Callejón, 2016). However, these methods require extensive sample pre-treatment and expensive equipment. Chemically modified electrodes are an interesting alternative to these analytical methods, since they do not require such specialized instrumentation, and do not need sample clean-up or derivatisation procedures, analyses thus being, in general, less time-consuming.

Another attractive alternative for Tyr determination is the use of biosensors, which combine biological recognition through enzyme specificity with the simplicity of construction. Biosensors based on tyrosinase (Tyr_{ase}) have been demonstrated to be sensitive for phenols determination, for example (Arecchi, Scampicchio, Drusch, & Mannino, 2010; Fiorentino, Gallone, Fiocco, Palazzo, & Mallardi, 2010; Nurul Karim & Lee, 2013; Yang, Xiong, Zhang, & Wang, 2012).

Tyr_{ase} contains two copper active sites in its structure which are responsible for the enzyme existing in three oxidation states; it catalyses the o-hydroxylation of monophenols to guiacol and in a second step the oxidation of guaiacol to o-quinones. For this reason, electrochemical biosensors based on Tyr_{ase} for detection of phenolic compounds have often been used. e.g. (Lu et al., 2010; Wang, Zheng, He, & Sheng, 2013). However, there are only a few reports on tyramine determination by tyrosinase based biosensors in the literature (Apetrei & Apetrei, 2013,

* Corresponding author.
E-mail address: cbrett@ci.uc.pt (C.M.A. Brett).

https://doi.org/10.1016/j.foodchem.2018.12.104
Received 31 July 2018; Received in revised form 7 November 2018; Accepted 22 December 2018
Available online 03 January 2019
0308-8146/

2015; Batra, Lata, Devi, Yadav, & Pundir, 2012). Good biosensor performance is extremely dependent on how adequate and effective is the enzyme immobilization. Some of the common approaches based on conductive nanomaterials have been used for the immobilization of Tyr_{ase} onto various substrates including carbon nanotubes, graphene, conducting polymers and nanoparticles (Wang et al., 2013). The controlled synthesis of conducting polymers allows rational design and preparation of new, biologically sensitive systems, since they contribute significantly to the improvement of the electrochemical current response and lower the limit of detection (Ates, 2013; Barsan, Ghica, & Brett, 2014; Petrova, Romanova, Madjarova, Ivanova, & Tadjer, 2012).

Gold nanoparticles (AuNP) have also received great interest for application in biosensors, providing advantages such as better access to and availability of reaction sites, as well as an improvement of biosensor response by the increase of surface area to which the biocomponent can be attached. The use of AuNP in composites with other nanomaterials such as conducting polymers, carbon nanotubes and graphene, has been shown to be an effective approach for electrode modification and enzyme immobilization for biosensor construction (Li, Schluesener, & Xu, 2010; Magar, Ghica, Abbas, & Brett, 2017; Singh, Jain, & Singla, 2013). In the present study, AuNP were synthesized using extracts of *Citrus sinensis* as both reducing and stabilizing agent. They were then incorporated in poly-(8-anilino-1-naphthalene sulphonic acid) (PANSA) by polymerization of the corresponding monomer in the presence of the AuNP. Following this, the enzyme Tyr_{ase} was immobilized over the nanocomposite and used for amperometric detection of Tyr. The dependence of the amperometric response, sensitivity, kinetics, linear range, limit of detection, stability, and selectivity was investigated. Finally, the prepared biosensor was applied to Tyr detection in fermented beverages (beer and red wine) and in dairy products (yogurt and Roquefort cheese).

2. Experimental

2.1. Reagents and solutions

The reagents were all of analytical grade and were used as received. Tyrosinase (Tyr_{ase}, from mushroom, activity 2687 U mg^{-1}, CAS number: 9002-10-2), bovine serum albumin (BSA) (2.0% w/v), glutaraldehyde (GA, 2.5% v/v in water), gold(III) chloride trihydrate ($HAuCl_4 \cdot 3H_2O$), 8-anilino-1-naphthalene sulphonic acid, 97% (ANSA) and tyramine 99.9% were acquired from Sigma-Aldrich. For the electrochemical experiments, the supporting electrolyte was Britton-Robinson (BR) buffer, prepared by mixing phosphoric acid, acetic acid and boric acid (all solutions of concentration 0.04 M) and adjusting the pH with 0.2 M sodium hydroxide solution. The stock solution of tyramine (Sigma-Aldrich) was prepared by dissolving the corresponding amount of compound in pure water. Xanthine (Sigma-Aldrich), hypoxanthine (Sigma-Aldrich), L-tyrosine hydrochloride (Sigma-Aldrich), dopamine hydrochloride (Sigma-Aldrich) were used for the interferent assessment.

Millipore Milli-Q nanopure water (resistivity ≥ 18 MΩ cm) was used for the preparation of all solutions. All experiments were performed at room temperature (25 ± 1 °C).

2.2. Instrumentation and measurements

Voltammetric and amperometric measurements were performed using a computer controlled IviumStat electrochemical analyser with IviumSoft version 2.024 software (Ivium Technologies, The Netherlands), in a one-compartment three-electrode system consisting of a glassy carbon electrode (GCE), area 0.00785 cm^2, bare or modified, as working electrode, a platinum wire counter electrode and an Ag/AgCl (3 M KCl) electrode as reference. A glass electrode pH meter model Crison Micro pH 2001 (Crison Instruments, S.A., Barcelona, Spain) was used for pH measurements. The XRD studies were carried out with an X-ray powder diffraction system (Siemens D5000, Bruker-AXS, Karlsruhe, Germany), Cu-Ka radiation ($(\lambda K\alpha_1 = 1.5406$ Å) in the 2θ range 0.5°–130°, operating voltage 40 kV and current 40 mA. A scanning electron microscope (SEM) (model JSM-5310, JEOL, Co., Japan) was used for examination of the AuNP, PANSA film and AuNP-PANSA nanocomposite film.

2.3. Green synthesis of gold nanoparticles (AuNP)

The gold nanoparticles were synthesized according to the literature (Sujitha & Kannan, 2013) with slight modifications. First, *C. sinensis* was squeezed to extract the juice which was then strained through a fine-mesh sieve. The filtered juice was centrifuged at 14,000 rpm for 30 min to remove all undesired impurities and to obtain a clear solution. For the synthesis of AuNP, 50 mL of 1 mM solution of gold (III) chloride trihydrate ($HAuCl_4 \cdot 3H_2O$) was brought to boil with vigorous stirring. A volume of 5 mL of previously purified juice extract of *C. sinensis* was added to this solution and allowed to cool slowly. The colour changed from yellow to colourless and then to ruby red, this whole process occurring within 5 min. The colloidal solution was stirred for a further 10 min whilst cooling to room temperature. The gold nanoparticle dispersion obtained was purified by repeated centrifugation at 14,000 rpm for 20 min followed by redispersion of the precipitated solid in 50 mL of Milli-Q water. The concentration of the resulting stock solution of gold nanoparticles was 197 mg L^{-1}.

2.4. Preparation of the electrode substrates for enzyme immobilization

The PANSA film was electrochemically synthesized from a solution containing 0.1 M ANSA monomer in 0.5 M H_2SO_4. For the preparation of AuNP-PANSA film, a more concentrated stock solution of the monomer in a higher concentration of H_2SO_4 was prepared and this solution was mixed in a ratio of 1:3 v/v with colloidal AuNP solution in order to obtain the same concentration of monomer and acid as that used for PANSA deposition. Oxygen inhibits polymer film growth; hence, in order to avoid its permeation, before polymerisation, the mixtures were degassed with N_2 for 20 min and during polymerisation, a flux of N_2 was kept flowing on top of the cell solution. The PANSA film and AuNP-PANSA film were grown on the GCE by potential cycling in the potential range 0.0 V–1.1 V vs Ag/AgCl using 50 mV s^{-1} as scan rate for 7 cycles, as previously optimised (Ngece et al., 2011). After polymerisation, the modified electrodes were carefully rinsed with Milli-Q water for removal of unreacted monomer and dried before enzyme immobilization. An AuNP/GCE modified electrode was also prepared by drop-casting 2 μL of AuNP colloidal solution on the GCE and left to dry for 1 h before enzyme immobilization.

2.5. Preparation of the biosensors

In order to optimize the amount of Tyr_{ase}, enzyme solutions were prepared by dissolving different amounts from 0.1 to 2.0% w/v of Tyr_{ase} in 0.1 M BR buffer (pH 7.0) containing BSA (2.0% w/v). In order to prepare the tyrosinase biosensors, 1 μL of the corresponding enzyme/BSA solution was mixed with 1 μL of GA (2.5% v/v) as crosslinking agent. The mixture was dropped onto the GCE, AuNP/GCE, PANSA/GCE and AuNP-PANSA/GCE surface and then left to react at room temperature (Ghica, Pauliukaite, Fatibello-Filho, & Brett, 2009). After drying, the biosensors were immersed in buffer (pH 7.0) for at least 2 h before use.

2.6. Real sample preparation and analysis

In order to evaluate the applicability of the new biosensor configuration in real sample analysis, the Tyr concentration was measured in two drinks that undergo a fermentation process during fabrication (red wine and beer) and two dairy products (yogurt and Roquefort cheese)

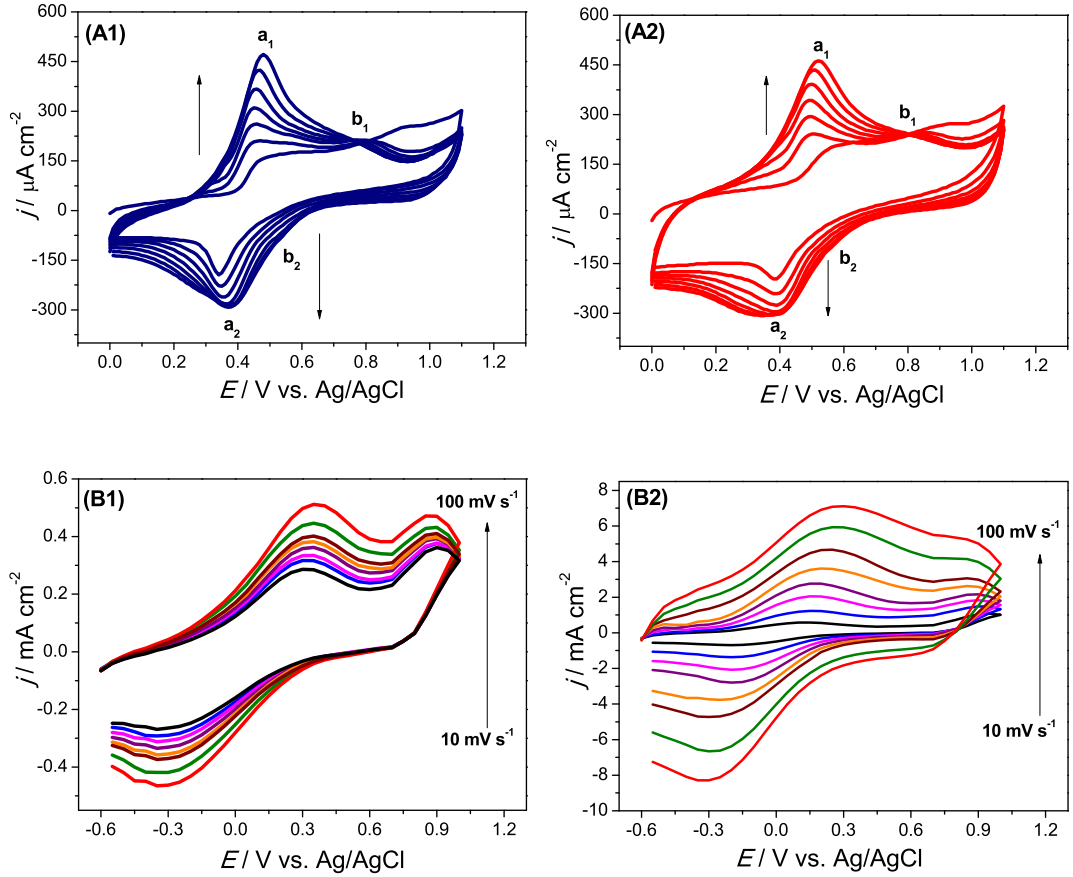

Fig. 1. Cyclic voltammetry for (A) electrochemical synthesis on GCE in 0.5 M H_2SO_4 of (A1) PANSA (A2) AuNP-PANSA, (B) 100 μM Tyr in 0.1 BR buffer (pH 7.0), scan rates 10–100 mV s^{-1}, at (B1) Tyr_{ase}/PANSA/GCE (B2) Tyr_{ase}/AuNP-PANSA/GCE.

using the standard addition method. The samples were prepared as described below.

The drinks were not diluted or pre-treated, except that the beer was degassed for 10 min before analysis. For both yogurt and Roquefort cheese, 2.5 g was accurately weighed and placed in a 50 mL volumetric flask and 20 mL of 0.1 M BR buffer (pH 7.0) was added. For solution homogenization, centrifugation was performed at 14,000 rpm during 20 min, then the supernatants were collected and kept at 4 °C before use.

3. Results and discussion

3.1. Synthesis of poly-(8-anilino-1-naphthalene sulphonic acid) and gold nanoparticle doped-poly-(8-aniline-1-naphthalene sulphonic acid) film on GCE

The growth profiles of PANSA and the nanocomposite AuNP-PANSA films electrodeposited on GCE are shown in Fig. 1A and 1B, respectively. Both possess two redox couples with similar voltammetric profiles to aniline polymerization (Chen et al., 2017; Marchesi, Jacumasso, Quintanilha, Winnischofer, & Vidotti, 2015; Milczarek, 2009). ANSA is an *N*-substituted aniline which has naphthalene sulphonic acid as a substituent in the amine ring. The redox couples a_1/a_2 and b_1/b_2 are attributed to intrinsic redox processes during polymer formation. The couple a_1/a_2 is the result of the transformation of aniline in ANSA from the reduced leucoemeraldine state to the partly oxidized emeraldine state. The second redox couple, b_1/b_2, is due to the transition of emeraldine to the pernigraniline state, which is accompanied by oxidation of ANSA (Iwuoha et al., 2006; Lindfors & Ivaska, 2002). The two anodic and two cathodic peaks which appeared at the initial stage of polymerization gradually merged into one redox couple (one anodic and one cathodic peak). The anodic peak current increased gradually with each cycle, while the cathodic peak stabilised after the 5th cycle. This behaviour indicates the self-limiting character of PANSA growth at higher cycle numbers. This is in agreement with other work, in which it was observed that the electropolymerization of aniline often has a self-accelerating character (Fang et al., 2015), while the naphthalene sulphonic acid moiety limits the rate of polymerization (Mažeikiene, Niaura, & Malinauskas, 2006). The mid-point potential between anodic and cathodic peaks for the polymer and the nanocomposite almost do not vary between the 2nd and 7th scan (~0.44 V vs. Ag/AgCl). However, an increase in peak separation occurs after the 5th cycle for both PANSA and AuNP-PANSA. The polymer growth voltammetric profile was very similar in the two cases, and was expressed as the ratio of the oxidation peak current in the seventh compared to the first cycle. For PANSA this factor was 3.21, while for AuNP-PANSA it was 3.14; the first cycle oxidation peak currents were also almost the same, see Fig. 1. Thus, the addition of AuNP to the monomer solution did not significantly affect the polymer growth rate. However, the inclusion of AuNP in the polymer matrix was beneficial for tyramine determination as explained below.

3.2. Characterization of the nanostructures

3.2.1. X-ray diffraction of the AuNP

The AuNP were examined by X-ray diffraction (XRD), Fig. 2A. The diffractograms show the XRD pattern of gold nanoparticles obtained from gold colloidal solution with Bragg reflection peaks at 36.4°, 44.3°, 64.9° and 77.8° in the 2θ range between 30° and 90° which can be indexed to (1 1 1), (2 0 0), (2 2 0) and (3 0 0) planes respectively in agreement with the face-centred cubic (fcc) gold crystal structure (Joint Committee on Power Diffraction Standards - JCPDS, 04-0784). The

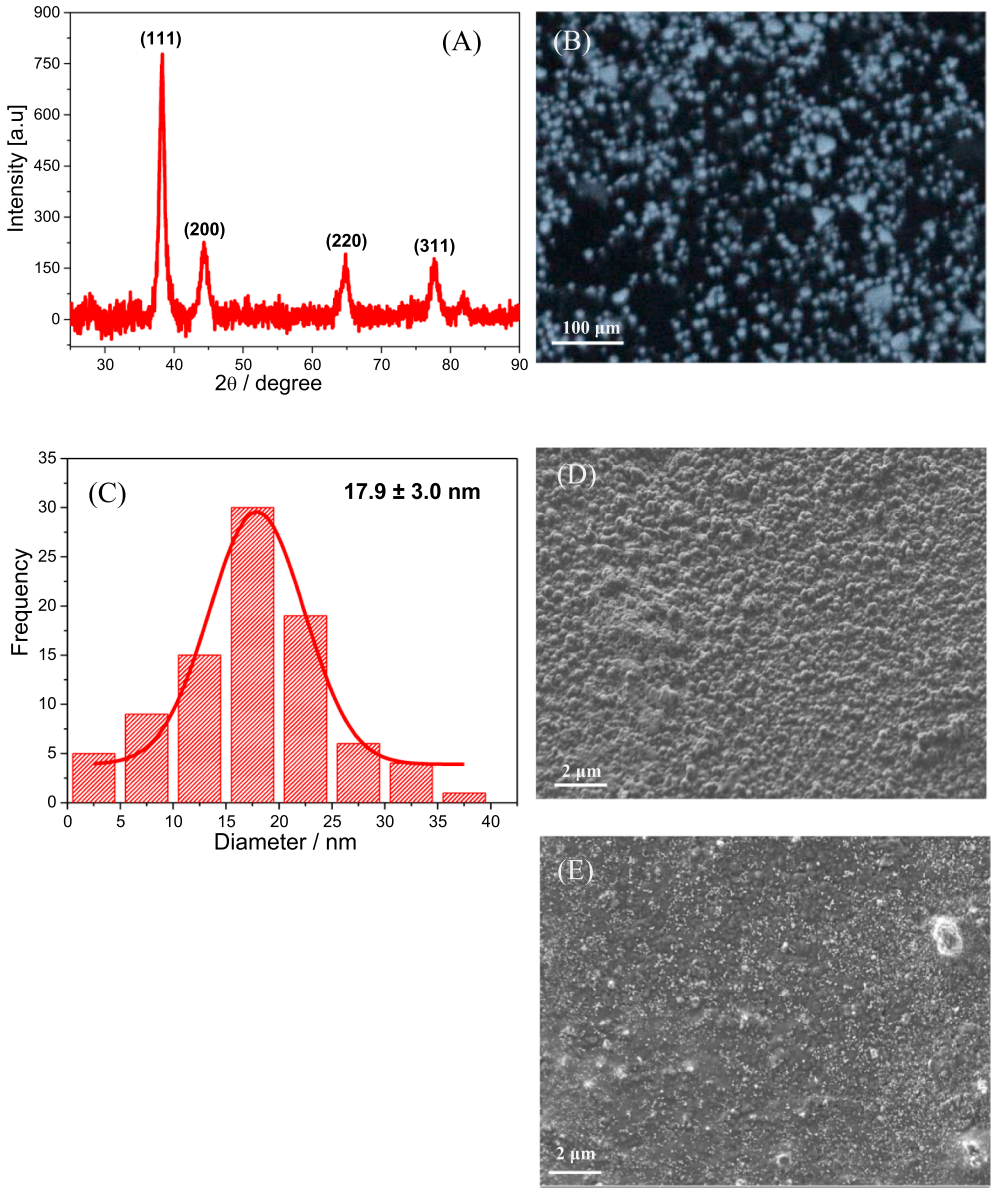

Fig. 2. (A) X-ray diffraction pattern recorded from drop-coated films of the colloid solution of gold nanoparticles synthesized with extract of *Citrus sinensis* on glass substrates. The Bragg reflections are identified in the XRD pattern (B) Scanning electron microscopy (SEM) of the nanoparticles (C) Gold nanoparticles diameter histogram (vertical bars) fitted with a Gaussian curve (D) SEM of the PANSA film (E) SEM of the AuNP-PANSA nanocomposite.

well-defined and intense peaks revealed that the AuNP was successfully synthesised by the reduction of Au^{+} using *C. sinensis* extracts, and shows its crystalline nature (Khademi-Azandehi & Moghaddam, 2015; Khan et al., 2017; Suresh et al., 2011). The mechanism for the thermal reduction of $HAuCl_4$ by citric acid from *C. sinensis* to form AuNP involves nucleation and growth processes. As shown in (Supplementary Material, Fig. S1), the coordination of citric acid with $Au^{III}Cl_4^-$ produces citrate–$Au^{III}Cl_3^-$ complexes which are activated thermostatically by a constant heating of the mixture producing a reduced $Au^{II}Cl_n^{m-}$ species, along with the formation of oxidation products of citric acid such as acetoacetate, CO_2, and dicarboxyacetone. Following this, the subsequent reduction of citrate-$Au^{II}Cl_n^{m-}$ and citrate-$Au^{I}Cl_n^{m-}$ complexes produce Au^0 and Au^0 nuclei, leading to the formation of AuNP. Citrate anions are adsorbed on the AuNP surface and act as surface-stabilising agent of the nanoparticle. The negative charge of citrate suppresses AuNP aggregation and leads to a more homogeneous dispersion of the nanoparticles, due to electrostatic repulsion (Shiraishi, Tanaka, Sakamoto, Ichikawa, & Hirai, 2017).

3.2.2. SEM of the nanostructures

The morphology of the AuNP, formed by the green synthesis method, was examined by scanning electron microscopy (SEM), as shown in Fig. 2B. SEM reveals the predominant presence of spherical and quasi-spherical like-shaped gold nanoparticles with a relatively well-dispersed distribution. The AuNP were analysed by ImageJ open source particle analysis software, in which 100 discreet and well-defined nanoparticles were used as sample space to measure the average size of the nanoparticles. From the Gaussian fitting curve to the histogram, Fig. 1C, the size of the nanoparticles was calculated to be 17.9 ± 3.0 nm. Similar results are found in the literature. Spherical gold nanoparticles of 30–50 nm diameter were achieved using *Penicillium* sp. (Du, Xian, & Feng, 2011), predominantly spherically-shaped gold nanoparticles ranging from 20 nm were synthesized using biodegradable green surfactants such as VeruSOL-3 (Nadagouda, Hoag, Collins, & Varma, 2009), quasi-spherical gold nanoparticles with diameter around 16 nm were obtained using the flower extract of *Rosa damascena* as a reducing and stabilizing agent (Ghoreishi, Behpour, & Khayatkashani, 2011).

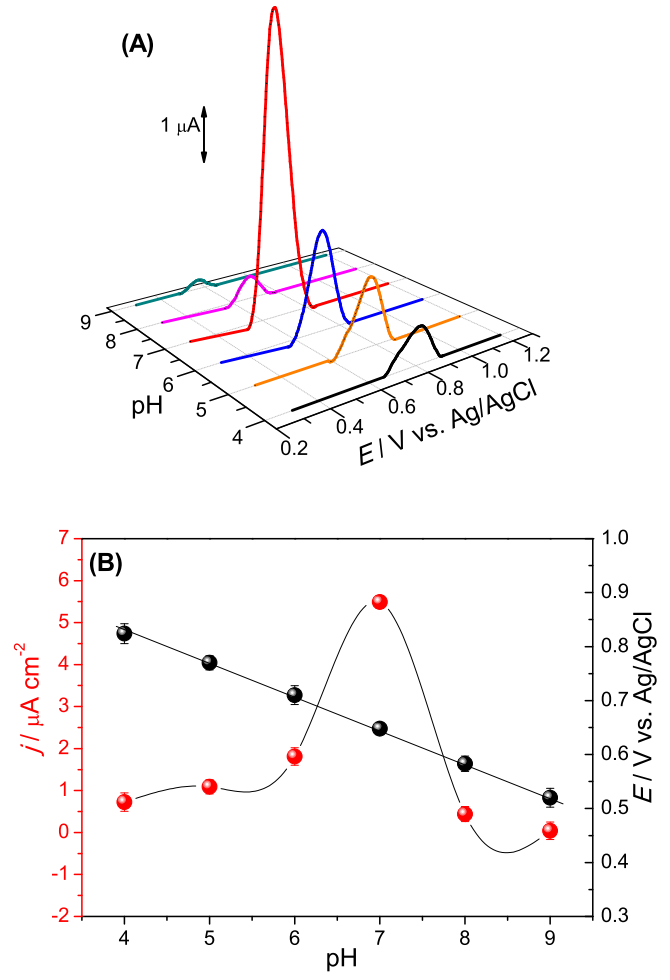

Fig. 3. (A) Differential pulse voltammograms of 100 μM Tyr at Tyr_{ase}/AuNP-PANSA/CGE in 0.1 M BR buffer at different pH values; (B) Effect of pH on the Tyr oxidation peak current and peak potential. The error bars correspond to measurements carried out with three different biosensors.

The surface morphologies of the PANSA and of the AuNP-PANSA nanocomposites are presented in the SEM images in Fig. 2D and E, respectively. For both coatings, there is a rough fully-covered surface with a uniform distribution of the polymer network and globular-like formations. Evidence of the uniform distribution of the nanoparticles in the polymer network was also seen by the presence of small spherical white spots (Fig. 2E) over the whole surface. Polymers are known to stabilize metal nanoparticles mainly by charge transfer interactions between the metal particles and the functional groups of heteroatoms on the polymer network (Dimitriev, 2004). In the case of PANSA, a derivative of polyaniline, the aggregation and stabilization of AuNP in the polymer network is controlled by the electrostatic attraction between protonated amines in the polymer film and the negative charge of the nanoparticle citrate capping groups. This stabilization of the AuNP in the polymer matrix prevents their leaching when the modified electrode is immersed in solution. Thus, this new methodology successfully incorporates nanoparticles in the polymer network through polymerization of the corresponding monomer in the presence of gold nanoparticles in solution.

3.3. Characterization of the biosensor in the presence of Tyr

The biosensor constructed by immobilisation of tyrosinase on the AuNP-PANSA modified electrode was characterised by cyclic voltammetry and differential pulse voltammetry in the presence of tyramine, investigating the influence of scan rate and of pH dependence.

3.3.1. Cyclic voltammetry – scan rate dependence

The influence of scan rate on biosensor response was investigated by recording cyclic voltammograms at the Tyr_{ase}/PANSA/GCE and Tyr_{ase}/AuNP-PANSA/GCE biosensors in 100 μM Tyr in 0.1 M BR buffer, pH 7.0 at different scan rates, from 10 to 100 mV s^{-1}, Fig. 2C and D respectively. The CVs at the modified electrodes showed that the electrode reaction was quasi-reversible and the Tyr_{ase}/AuNP-PANSA/GCE biosensor presents a higher peak current at all scan rates evaluated.

The values of redox peak current densities j_{pa} and j_{pc}, expressed in mA cm^{-2}, are linearly proportional to the scan rate (not shown) in both cases, according to:

Tyr_{ase}/PANSA/GCE: $j_{pa} = 0.0013\nu + 0.11$, $r = 0.9997$, $j_{pc} = -0.0023\nu - 0.0013$, $r = 0.9995$

Tyr_{ase}/AuNP-PANSA/GCE: $j_{pa} = 0.033 \quad \nu + 0.29$, $r = 0.9983$; $j_{pc} = -0.042\ \nu + 0.0064$, $r = 0.9984$

The relationship log j_{pa} versus log ν (not shown) had slopes of 0.89 for Tyr_{ase}/PANSA/GCE and 0.98 for Tyr_{ase}/AuNP-PANSA/GCE, close to the theoretical value of 1.0 characteristic of an adsorption-controlled process, whereas for diffusion-controlled processes the slope would be 0.5 (Brett & Oliveira-Brett, 1993).

A linear relationship between E_p and log ν was also obtained. For an adsorption-controlled process, the electron transfer coefficient (α) can be calculated from the relationship (E_{pa} or E_{pc}) and log ν using Laviron's model (Laviron, 1979). The linear regression equation obtained from the plot of E_{pa} vs log ν (not shown) for Tyr_{ase}/AuNP-PANSA/GCE is:

$$E_{pa} = 0.070 \log \nu + 0.069 \quad r = 0.9967$$

For Tyr_{ase}/PANSA/GCE the corresponding equation is:

$$E_{pa} = 0.060 \log \nu + 0.25 \quad r = 0.9969$$

According to Laviron's equations, the slope is equal to $2.3\,RT/\alpha_a nF$ for the anodic peak and can be used to evaluate the value of α_a, the electron transfer coefficient for Tyr oxidation. Here R is the ideal gas constant, T is the temperature (K), F is the Faraday constant, and n is the number of electrons involved in the redox process. Since Tyr oxidation involves two electrons, the value of α_a for Tyr_{ase}/AuNP-PANSA/GCE was estimated to be 0.42 and for Tyr_{ase}/PANSA/GCE it was 0.49. These values are within the range expected.

3.3.2. Differential pulse voltammetry – influence of pH

The literature reports that the enzymatic activity of Tyr_{ase} is lost below pH 4.0 and above pH 9.0 (Tan, Kan, & Li, 2011; Vicentini, Janegitz, Brett, & Fatibello-Filho, 2013); hence the influence of solution pH on the oxidation of 100 μM Tyr was investigated by DPV in the pH range from 4.0 to 9.0. As can be seen in Fig. 3A, the maximum oxidation peak current was obtained at pH 7.0. Therefore, this pH was selected as optimum pH and used in Tyr determination. With increasing solution pH from 4.0 to 9.0, the oxidation peak potential shifted negatively and linearly, Fig. 3B, according to E_{pa} (V) = 1.06 − 0.060 pH with a correlation coefficient of 0.9987, the slope being close to the theoretical value of 59 mV pH^{-1} at 25 °C for an electrode process involving equal number of protons and electrons. The peak width at half height, $W_{1/2} = 3.52\,RT/nF$, where R is the universal gas constant, T the temperature in K, and F the Faraday constant gives an indication of the reversibility of the electrode reaction and the number of electrons involved. The minimum peak width for a reversible one-electron process is 90 mV and for a reversible two-electron process is 45 mV (Brett & Oliveira-Brett, 1993). In this work, see Fig. 3A, $W1_{/2}$ was approximately 45 mV over the pH range studied, therefore, can be assumed that two electrons are involved in the reaction (Apetrei & Apetrei, 2013,

2015) as proposed in the mechanism described in the following section.

3.4. Optimization of the amperometric biosensor

The analytical determination of Tyr was performed by fixed potential amperometry and in order to optimize the response, the effect of the applied potential and enzyme loading were investigated.

3.4.1. Influence of the applied potential

The applied potential has a big influence on biosensor performance since it contributes to its sensitivity and selectivity. The biosensor response to 100 μM Tyr in 0.1 M BR buffer (pH 7.0) was studied between −0.5 and +0.3 V vs. Ag/AgCl. The current increases rapidly as the potential becomes less negative from −0.5 to −0.3 V, with a maximum at −0.3 V and then decreases up to −0.1 V, above which the response is almost constant.

Tyr_{ase} catalyses the hydroxylation of Tyr (Eq. (1)) as well as the oxidative conversion of the resulting dopamine to *o*-dopaquinone (Eq. (2)). The enzymatically generated o-dopaquinone by-product can easily undergo electrochemical reduction at a potential close to 0.0 V (Apetrei & Apetrei, 2013, 2015) (Eq. (3)). This reaction is verified in CVs (Fig. 2B) since a reduction peak appears at a potential close to −0.3 V in the presence of Tyr (Njagi, Chernov, Leiter, & Andreescu, 2010). The sensing principle of the biosensor is based on measuring the increase of the cathodic amperometric signal related to the electrochemical reduction of *o*-dopaquinone enzymatically generated on the biosensor surface that involves 2 electrons and 2 protons.

$$\text{Tyramine} + 1/2O_2 \xrightarrow{\text{tyrosinase}} \text{Dopamine} \quad (1)$$

$$\text{Dopamine} + 1/2O_2 \xrightarrow{\text{tyrosinase}} \text{o} - \text{Dopaquinone} + H_2O \quad (2)$$

$$\text{o} - \text{Dopaquinone} + 2H^+ + 2e^- \xrightarrow{\text{tyrosinase}} \text{Dopamine} + H_2O \quad (3)$$

Independent cyclic voltammetry measurements at tyrosinase modified glassy carbon electrodes at pH 7.0 with the addition of dopamine or tyramine were done (Supplementary Material, Fig. S2). In the presence of dopamine, two redox couples appear with midpoint potentials −0.160 V and +0.250 V; the couple I at more positive potentials is ascribed to dopamine/dopaquinone and the more negative one, II, to dopaquinone reduction. With tyramine only, an additional anodic peak III_a appears, corresponding to irreversible tyramine oxidation. The redox couples I and II are present except that both cathodic peaks are ca. 0.20 V more negative. Thus, as can be seen, the reduction of dopaquinone occurs at −0.3 V.

In cyclic voltammetry at Tyr_{ase}/AuNP-PANSA/GCE or Tyr_{ase}/PANSA/GCE, the adsorption of tyramine and its oxidation products in the modifier films led to a very broad redox couple and it was not possible to distinguish the processes. However, the determination of tyramine by fixed potential amperometry was carried out successfully and with better analytical parameters at the Tyr_{ase}/AuNP-PANSA/GCE biosensor than without the presence of AuNP-PANSA nanocomposite, see Section 3.5.1.

In the light of the results obtained, an applied potential of −0.30 V was selected to be used in further experiments for Tyr determination. Moreover, this potential, close to 0.0 V, minimizes the likelihood of potential interferences from common electroactive species.

3.4.2. Effect of the amount of tyrosinase

In order to determine the optimal amount of Tyr_{ase} immobilized on AuNP-PANSA/GCE for Tyr determination, different Tyr_{ase} loadings ranging from 0.1 to 3.5% (w/v) were tested, the concentrations of GA and BSA being fixed at 2.5% (v/v) and 2.0% (v/v) respectively. The amperometric response to 100 μM Tyr was tested for different enzyme loadings, using the same experimental conditions. The cathodic current increases as the amount of Tyr_{ase} is increased, reaching a maximum for 2.0% (w/v) of Tyr_{ase}. For higher loadings, there is a decrease in biosensor sensitivity. This indicates that high amounts of enzyme compromise biosensor performance, this being attributable to diffusion limitations and to a too low concentration of dissolved oxygen, a natural cofactor for enzyme regeneration (Lu et al., 2010). Therefore, 2.0% (w/v) of the enzyme was chosen as the best for biosensor construction.

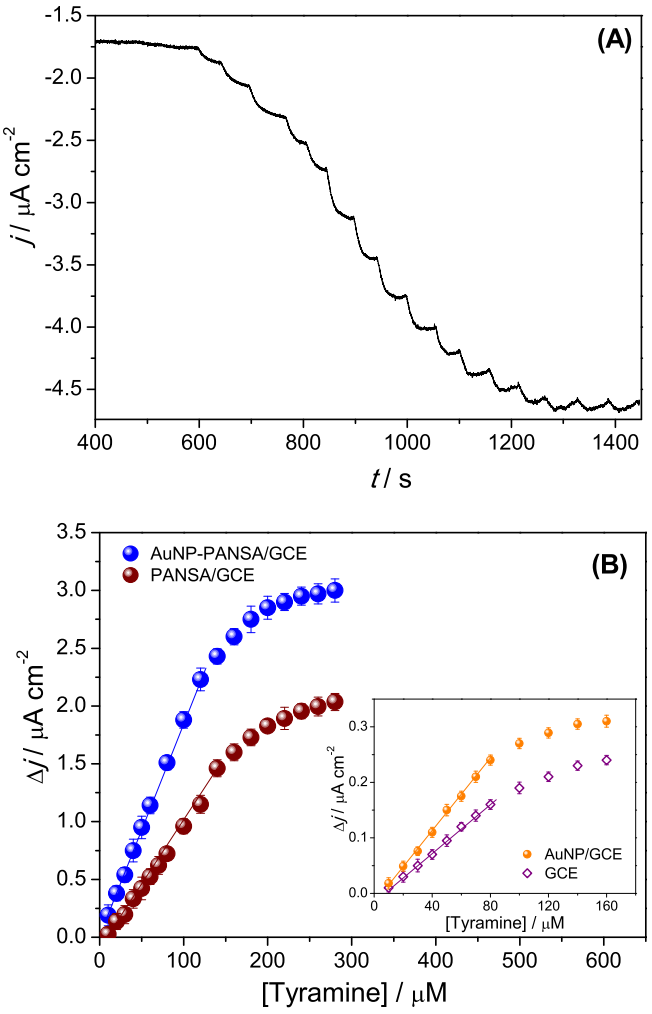

Fig. 4. (A) Amperometric response of Tyr_{ase}/AuNP-PANSA/CGE biosensor to tyramine in 0.1 M BR buffer (pH 7.0); (B) Calibration curves for tyramine in 0.1 M BR buffer (pH 7.0) at −0.30 V for GCE, AuNP/GCE, PANSA/GCE and AuNP-PANSA/GCE. The error bars are calculated from measurements carried out with three different biosensors.

3.5. Amperometric biosensor for tyramine

3.5.1. Analytical performance

The amperometric responses of Tyr_{ase}/AuNP-PANSA/GCE, Tyr_{ase}/PANSA/GCE, Tyr_{ase}/AuNP/GCE and, Tyr_{ase}/GCE biosensors for Tyr determination under the optimized conditions were evaluated. The biosensors show a rapid bioelectrocatalytic response, reaching 95% of the steady-state current within 8 s after each Tyr addition. Fig. 4A is a representative chronoamperometric profile for Tyr determination, showing a linear increase of the change in cathodic current with Tyr concentration for all the biosensor assemblies tested. Fig. 4B displays the calibration plots obtained from the amperometric responses. The Tyr_{ase}/AuNP-PANSA/GCE biosensor presents the highest sensitivity of 19 nA cm^{-2} μM^{-1} and lowest limit of detection (LoD) of 0.7 μM, following the linear regression equation: Δj (μA cm^{-2}) = $-3.58 \times 10^{-3} + 1.90 \times 10^{-2}$ [Tyr] (μM), with a correlation

coefficient (R^2) equal to 0.9987. For the Tyr_{ase}/PANSA/GCE biosensor, the sensitivity was calculated to be 10 nA cm^{-2} μM^{-1} and the LoD was 1.35 μM, where Δj (μA cm^{-2}) = $-0.10 + 1.0 \times 10^{-2}$ [Tyr] μM, (R^2 = 0.9985). The Tyr_{ase}/AuNP/GCE biosensor presented a sensitivity of 3.20 nA cm^{-2} μM^{-1} and LoD of 2.91 μM, with Δj (μA cm^{-2}) = $-0.016 + 3.2 \times 10^{-3}$ [Tyr] μM, (R^2 = 0.9987). Finally, the Tyr_{ase}/GCE biosensor had the lowest sensitivity of 1.20 nA cm^{-2} μM^{-1} and highest LoD of 3.98 μM, where Δj (μA cm^{-2}) = $-0.014 + 1.2 \times 10^{-3}$ [Tyr] μM, (R^2 = 0.9987).

In order to evaluate the binding affinity of the immobilized enzyme (Tyr_{ase}) with its substrate Tyr, the Hill constant, h, was estimated from the slope of the relationship of log (I/I_{max}) versus log [Tyr] using the values obtained in the calibration curves. For non-cooperative binding, the Hill constant is equal to 1.0; values of $h < 1$ indicate negative cooperative binding; this means that the binding of ligand makes further binding more difficult. Positive cooperativity is reflected in values of $h > 1$, meaning that binding of ligand makes further binding easier. From the Hill plot, the slopes for Tyr_{ase}/AuNP-PANSA/GCE, Tyr_{ase}/PANSA/GCE, Tyr_{ase}/AuNP/GCE and Tyr_{ase}/GCE biosensors were calculated to be 1.43, 1.13, 0.89 and 0.76, respectively, which indicate a strong affinity between Tyr_{ase} and Tyr at the new modified electrode support (AuNP-PANSA/GCE). This result indicates that the reaction between the enzyme and the target analyte (Tyr) has Michaelis-Menten type kinetics, as suggested previously (Berg, Tymoczko, & Stryer, 2006; Feher, 2012). The Michaelis-Menten constant for Tyr_{ase} /AuNP-PANSA/GCE was estimated to be 79.3 μM, a similar value to those obtained by Apetrei and Apetrei (2013) (62.65 μM) and Apetrei and Apetrei (2015) (88.52 μM).

A comparison of the electroanalytical properties of recently reported Tyr sensors is summarized in Table 1. The detection limit of the new platform, Tyr_{ase}/AuNP-PANSA/GCE was similar or lower than that of other reported biosensors. The same observation can be made for the linear range of the developed biosensor. Besides this, the novel Tyr_{ase}/AuNP-PANSA/GCE has several advantages, such as easy and rapid electrode modification, as well as a lower limit of detection and applied potential, compared with other biosensors for Tyr detection that have more complex architectures, see Table 1.

3.5.2. Repeatability and stability of Tyr_{ase}/AuNP-PANSA/GCE biosensor

The repeatability of the Tyr_{ase}/AuNP-PANSA/GCE biosensor was investigated by amperometrically measuring the response to 100 μM Tyr (BR, pH 7.0). After 20 successive assays the current was 97.5% of the initial value (RSD = 4.3%, n = 3). When not in use the biosensors were kept in buffer (BR, pH 7.0) at 4 °C. After 20 days, the amperometric response of the biosensor for Tyr determination was 94.3% (RSD = 4.3%, n = 3) of the original, showing that the biosensor has a favourable long-term stability, comparable to those reported in the literature (Apetrei & Apetrei, 2013, 2015; Kochana et al., 2016).

3.5.3. Interference studies

Selectivity, a very important parameter for application to real samples, was evaluated amperometrically at −0.30 V fixed potential by the sequential addition of possible interferents after the initial addition of 100 μM Tyr. The interferents added were xanthine (100 μM), hypoxanthine (100 μM), L-tyrosine (100 μM) and dopamine (100 μM) after which a second addition of Tyr was made. The compounds xanthine, hypoxanthine, and L-tyrosine led to a change in the current of less than 2%. Dopamine presented a reduction in current similar to Tyr, which is to be expected since it is converted to o-dopaquinone by tyrosinase. However, dopamine is not normally present in food products, the object of application of the present biosensor. For the second addition of Tyr, there was no significant change in the current response, compared with the first addition.

3.5.4. Determination of tyramine in food and beverages

In order to illustrate the practical and potential applications of the biosensor proposed, a variety of commercial food samples including yogurt, Roquefort cheese, red wine and beer were purchased from a local supermarket to evaluate the presence of Tyr. Amperometric measurements under optimal experimental conditions were applied for the quantification. Each sample was measured in triplicate, using the standard addition method, in order to minimise the matrix effect when analysing complex samples. The quantity of Tyr found in the original samples is given as the value obtained in the cell after dilution; which was 1:20 for dairy foods and 1:100 for fermented drinks. The results are given in Table 2. It was calculated that Roquefort cheese and yogurt contained 62.7 mg L^{-1} and 3.07 mg L^{-1} while red wine and beer contained 7.98 mg L^{-1} and 9.65 mg L^{-1}, the values achieved being in agreement with those expected (Mayr & Schieberle, 2012; Novella-Rodríguez, Veciana-Nogués, Izquierdo-Pulido, & Vidal-Ca, 2003; Ordóñez et al., 2016). The recoveries were in the range from 93% to 97% with RSDs less than 2.5%, indicating that the proposed method is appropriate for practical applications in food safety control with an acceptable level of reliability.

Table 1
Comparative performance of different biosensor configurations for tyramine determination.

Modified electrode configuration	Principle of detection	Applied potential/ V	Linear range/ μM	LOD/μM	K_M/μM	Ref
Tyr_{ase}/PO_4-PPy/PtE	Amperometry	−0.25 (Ag/AgCl)	4.0–80	0.57	62.6	(Apetrei & Apetrei, 2013)
Tyr_{ase}–SWCNT–COOH/SPE	Amperometry	−0.20 (SPE)	5.0–180	0.62	88.5	(Apetrei & Apetrei, 2015)
TyOx/AgNP/L-Cys/AuE	Amperometry	+0.25 (Ag/AgCl)	17–250	10.0	–	(Batra et al., 2012)
PSAO-Nafion/MgO_2/CPE	Amperometry	+0.40 (Ag/AgCl)	10–300	3.0	–	(Telsnig et al., 2012)
Tyr_{ase}/TiO_2/CMK-3/PDDA/Nafion/GE	Cyclic voltammetry	–	6.0–130	1.5	66	(Kochana et al., 2016)
$SPC_{HRP}E$	Amperometry	0.0 (SPCE)	2.0–456	2.1	–	(Calvo-Pérez, Domínguez-Renedo, Alonso-Lomillo, & Arcos-Martínez, 2013b)
HRP/SPCE		0.0 (SPCE)	0.2–21.4	0.2	–	
PAO/HOMFc/SPCE	Amperometry	+0.26 (Ag/AgCl)	2.0–164	2.0	–	(Calvo-Pérez, Domínguez-Renedo, Alonso-Lomillo, & Arcos-Martínez, 2013a)
Tyr_{ase}/AuNP-PANSA/GCE	Amperometry	−0.30 (Ag/AgCl)	10–120	0.71	79.3	This work

Tyr_{ase}/PO_4-Ppy/PtE - tyrosinase/polypyrrole doped with phosphate ions on platinum disk electrode; Tyr_{ase}–SWCNT–COOH/SPE - screen-printed carbon electrodes modified with carboxyl functionalized Single-Walled Carbon Nanotubes; TyOx/AgNPs/L-Cys/AuE - tyramine oxidase onto citric acid-capped silver nanoparticles bound to surface of Au electrode through cysteine self-assembled monolayer; PSAO-Nafion/MgO_2CPE- Pea seedling amine oxidase immobilized with nafion on carbon paste modified with manganese dioxide as mediator; Tyr_{ase}/TiO_2/CMK-3/PDDA/Nafion/GE - Tyrosinase immobilized into mesoporous carbon CMK-3, titania dioxide sol, poly(diallyldimethylammonium chloride) and Nafion onto graphite electrode; PAO/HOMFc/SPCE - plasma amino oxidase immobilized on screen printed carbon electrode using hidroxymethylferrocene as mediator.

Table 2
Determination of tyramine in fermented drink and dairy products.

Sample	Determined (μM)	Added (μM)	Expected (μM)	Found (μM)	RSD (%)	Recovery (%)
Yogurt	0.22	2.00	2.22	2.15	4.44	96.8
Roquefort cheese	4.57	2.00	6.57	6.38	3.19	97.1
Red wine	1.46	2.00	3.46	3.22	4.18	93.1
Beer	1.82	2.00	3.82	3.67	4.67	96.1

4. Conclusions

A novel biosensor configuration based on Tyr_{ase}/AuNP-PANSA/GCE for tyramine determination that is easy to construct, and is rapid and sensitive is proposed. The new biosensor exhibited a low limit of detection and a wide linear range, similar to values found for more complex architectures. From the Hill constant $h > 1$, a strong interaction between the enzyme and the electrode substrate was revealed, as well as a Michaelis-Menten profile. The developed biosensor showed good selectivity, stability, repeatability, and has been successfully applied to determine tyramine in commercial food products with good recoveries, auguring well for its use in food safety control.

The authors declare that they have no conflict of interest.

Acknowledgements

The authors thank Fundação para a Ciência e a Tecnologia (FCT), Portugal, projects PTDC/QEQ-QAN/2201/2014, in the framework of Project 3599-PPCDT, and UID/EMS/00285/2013 (both co-financed by the European Community Fund FEDER) and the European Union Marie Curie International Research Staff Exchange Scheme (IRSES), project SmartCancerSens PIRSES-GA-2012-318053, for financial support. MEG thanks FCT for a postdoctoral fellowship SFRH/BPD/103103/2014 and WS thanks the Conselho Nacional de Desenvolvimento Científico e Tecnológico (CNPq), Brazil for a doctoral fellowship, 232979/2014-6.

Appendix A. Supplementary data

Supplementary data to this article can be found online at https://doi.org/10.1016/j.foodchem.2018.12.104.

References

Apetrei, I. M., & Apetrei, C. (2013). Amperometric biosensor based on polypyrrole and tyrosinase for the detection of tyramine in food samples. *Sensors and Actuators, B: Chemical, 178*, 40–46. https://doi.org/10.1016/j.snb.2012.12.064.

Apetrei, I. M., & Apetrei, C. (2015). The biocomposite screen-printed biosensor based on immobilization of tyrosinase onto the carboxyl functionalised carbon nanotube for assaying tyramine in fish products. *Journal of Food Engineering, 149*, 1–8. https://doi.org/10.1016/j.jfoodeng.2014.09.036.

Arecchi, A., Scampicchio, M., Drusch, S., & Mannino, S. (2010). Nanofibrous membrane based tyrosinase-biosensor for the detection of phenolic compounds. *Analytica Chimica Acta, 659*(1–2), 133–136. https://doi.org/10.1016/j.aca.2009.11.039.

Ates, M. (2013). A review study of (bio)sensor systems based on conducting polymers. *Materials Science and Engineering C*. https://doi.org/10.1016/j.msec.2013.01.035.

Atta, N. F., & Abdel-Mageed, A. M. (2009). Smart electrochemical sensor for some neurotransmitters using imprinted sol-gel films. *Talanta, 80*(2), 511–518. https://doi.org/10.1016/j.talanta.2009.07.014.

Bacaloni, A., Insogna, S., Sancini, A., Ciarrocca, M., & Sinibaldi, F. (2013). Sensitive profiling of biogenic amines in human urine by capillary electrophoresis with field amplified sample injection. *Biomedical Chromatography, 27*(8), 987–993. https://doi.org/10.1002/bmc.2891.

Barsan, M. M., Ghica, M. E., & Brett, C. M. A. (2014). Electrochemical sensors and biosensors based on redox polymer/carbon nanotube modified electrodes: A review. *Analytica Chimica Acta, 881*, 1–23. https://doi.org/10.1016/j.aca.2015.02.059.

Batra, B., Lata, S., Devi, R., Yadav, S., & Pundir, C. S. (2012). Fabrication of an amperometric tyramine biosensor based on immobilization of tyramine oxidase on AgNPs/l-Cys-modified Au electrode. *Journal of Solid State Electrochemistry, 16*(12), 3869–3876.

Berg, J. M., Tymoczko, J. L., & Stryer, L. (2006). Biochemistry (5th ed.). In: Biochemistry textbook (p. 1120). http://doi.org/10.1007/s13398-014-0173-7.2.

Brett, C. M. A., & Oliveira-Brett, A. M. (1993). *Electrochemistry: Principles, methods, and applications*. Oxford: Oxford Un iversity Press.

Calvo-Pérez, A., Domínguez-Renedo, O., Alonso-Lomillo, M. A., & Arcos-Martínez, M. J. (2013a). Disposable amperometric biosensor for the determination of tyramine using plasma amino oxidase. *Microchimica Acta, 180*(3–4), 253–259. https://doi.org/10.1007/s00604-012-0926-y.

Calvo-Pérez, A., Domínguez-Renedo, O., Alonso-Lomillo, M. A., & Arcos-Martínez, M. J. (2013b). Disposable horseradish peroxidase biosensors for the selective determination of tyramine. *Electroanalysis, 25*(5), 1316–1322. https://doi.org/10.1002/elan.201200636.

Chen, C., Gan, Z., Xu, C., Lu, L., Liu, Y., & Gao, Y. (2017). Electrosynthesis of poly(aniline-co-azure B) for aqueous rechargeable zinc-conducting polymer batteries. *Electrochimica Acta, 252*, 226–234. https://doi.org/10.1016/j.electacta.2017.08.195.

Cheng, M., Zhang, X., Wang, M., Huang, H., & Ma, J. (2017). A facile electrochemical sensor based on well-dispersed graphene-molybdenum disulfide modified electrode for highly sensitive detection of dopamine. *Journal of Electroanalytical Chemistry, 786*, 1–7. https://doi.org/10.1016/j.jelechem.2017.01.012.

Cinquina, A. L., Calì, A., Longo, F., De Santis, L., Severoni, A., & Abballe, F. (2004). Determination of biogenic amines in fish tissues by ion-exchange chromatography with conductivity detection. *Journal of Chromatography A, 1032*(1–2), 73–77. https://doi.org/10.1016/j.chroma.2004.01.013.

Dimitriev, O. P. (2004). Doping of polyaniline by transition-metal salts. *Macromolecules, 37*(9), 3388–3395. https://doi.org/10.1021/ma035677w.

Du, L., Xian, L., & Feng, J.-X. (2011). Rapid extra-/intracellular biosynthesis of gold nanoparticles by the fungus Penicillium sp. *Journal of Nanoparticle Research, 13*(3), 921–930.

Fang, Y., Jiang, Q., Deng, M., Tian, Y., Wen, Q., & Wang, M. (2015). Preparation in-situ of carbon nanotubes/polyaniline modified electrode and application for ascorbic acid detection. *Journal of Electroanalytical Chemistry, 755*, 39–46.

Feher, J. (2012). Quantitative human physiology. *Quantitative Human Physiology,* 270–280. https://doi.org/10.1016/B978-0-12-382163-8.00030-X.

Fiorentino, D., Gallone, A., Fiocco, D., Palazzo, G., & Mallardi, A. (2010). Mushroom tyrosinase in polyelectrolyte multilayers as an optical biosensor for o-diphenols. *Biosensors and Bioelectronics, 25*(9), 2033–2037. https://doi.org/10.1016/j.bios.2010.01.033.

Galgano, F., Favati, F., Bonadio, M., Lorusso, V., & Romano, P. (2009). Role of biogenic amines as index of freshness in beef meat packed with different biopolymeric materials. *Food Research International, 42*(8), 1147–1152. https://doi.org/10.1016/j.foodres.2009.05.012.

Ghica, M. E., Pauliukaite, R., Fatibello-Filho, O., & Brett, C. M. A. (2009). Application of functionalised carbon nanotubes immobilised into chitosan films in amperometric enzyme biosensors. *Sensors and Actuators, B: Chemical, 142*(1), 308–315. https://doi.org/10.1016/j.snb.2009.08.012.

Ghoreishi, S. M., Behpour, M., & Khayatkashani, M. (2011). Green synthesis of silver and gold nanoparticles using *Rosa damascena* and its primary application in electrochemistry. *Physica E: Low-Dimensional Systems and Nanostructures, 44*(1), 97–104. https://doi.org/10.1016/j.physe.2011.07.008.

Iwuoha, E. I., Mavundla, S. E., Somerset, V. S., Petrik, L. F., Klink, M. J., Sekota, M., & Bakers, P. (2006). Electrochemical and spectroscopic properties of fly ash-polyaniline matrix nanorod composites. *Microchimica Acta, 155*(3–4), 453–458. https://doi.org/10.1007/s00604-006-0584-z.

Khademi-Azandehi, P., & Moghaddam, J. (2015). Green synthesis, characterization and physiological stability of gold nanoparticles from *Stachys lavandulifolia* Vahl extract. *Particuology, 19*, 22–26. https://doi.org/10.1016/j.partic.2014.04.007.

Khan, F. U., Chen, Y., Khan, N. U., Ahmad, A., Tahir, K., Khan, Z. U. H., ... Wan, P. (2017). Visible light inactivation of *E. coli*, cytotoxicity and ROS determination of biochemically capped gold nanoparticles. *Microbial Pathogenesis, 107*, 419–424. https://doi.org/10.1016/j.micpath.2017.04.024.

Kochana, J., Wapiennik, K., Knihnicki, P., Pollap, A., Janus, P., Oszajca, M., & Kuśtrowski, P. (2016). Mesoporous carbon-containing voltammetric biosensor for determination of tyramine in food products. *Analytical and Bioanalytical Chemistry, 408*(19), 5199–5210. https://doi.org/10.1007/s00216-016-9612-y.

Laviron, E. (1979). General expression of the linear potential sweep voltammogram in the case of diffusionless electrochemical systems. *Journal of Electroanalytical Chemistry, 101*(1), 19–28. https://doi.org/10.1016/S0022-0728(79)80075-3.

Li, Y., Schluesener, H. J., & Xu, S. (2010). Gold nanoparticle-based biosensors. *Gold Bulletin, 43*(1), 29–41. https://doi.org/10.1007/BF03214964.

Lindfors, T., & Ivaska, A. (2002). Potentiometric and UV-vis characterisation of N-substituted polyanilines. *Journal of Electroanalytical Chemistry, 535*(1–2), 65–74. https://doi.org/10.1016/S0022-0728(02)01172-5.

Lu, L., Zhang, L., Zhang, X., Huan, S., Shen, G., & Yu, R. (2010). A novel tyrosinase biosensor based on hydroxyapatite-chitosan nanocomposite for the detection of phenolic compounds. *Analytica Chimica Acta, 665*(2), 146–151. https://doi.org/10.1016/j.aca.2010.03.033.

Magar, H. S., Ghica, M. E., Abbas, M. N., & Brett, C. M. A. (2017). A novel sensitive amperometric choline biosensor based on multiwalled carbon nanotubes and gold nanoparticles. *Talanta, 167*, 462–469. https://doi.org/10.1016/j.talanta.2017.02.

048.
Marchesi, L. F., Jacumasso, S. C., Quintanilha, R. C., Winnischofer, H., & Vidotti, M. (2015). The electrochemical impedance spectroscopy behavior of poly(aniline) nanocomposite electrodes modified by Layer-by-Layer deposition. *Electrochimica Acta, 174*, 864–870. https://doi.org/10.1016/j.electacta.2015.05.077.
Mayr, C. M., & Schieberle, P. (2012). Development of stable isotope dilution assays for the simultaneous quantitation of biogenic amines and polyamines in foods by LC-MS/MS. *Journal of Agricultural and Food Chemistry, 60*(12), 3026–3032. https://doi.org/10.1021/jf204900v.
Mažeikiene, R., Niaura, G., & Malinauskas, A. (2006). Raman spectroelectrochemical study of self-doped copolymers of aniline and selected aminonaphthalenesulfonates. *Electrochimica Acta, 51*(10), 1917–1924. https://doi.org/10.1016/j.electacta.2005.06.025.
Milczarek, G. (2009). Electrochemical conversion of poly-aniline into a redox polymer in the presence of nordihydroguaiaretic acid. *Journal of Electroanalytical Chemistry, 626*(1–2), 143–148. https://doi.org/10.1016/j.jelechem.2008.12.002.
Nadagouda, M. N., Hoag, G., Collins, J., & Varma, R. S. (2009). Green synthesis of Au nanostructures at room temperature using biodegradable plant surfactants. *Crystal Growth and Design, 9*(11), 4979–4983. https://doi.org/10.1021/cg9007685.
Ngece, R. F., West, N., Ndangili, P. M., Olowu, R. A., Williams, A., Hendricks, N., ... Iwuoha, E. (2011). A silver nanoparticle/poly (8-anilino-1-naphthalene sulphonic acid) bioelectrochemical biosensor system for the analytical determination of ethambutol. *International Journal of Electrochemical Science, 6*, 1820–1834.
Njagi, J., Chernov, M. M., Leiter, J. C., & Andreescu, S. (2010). Amperometric detection of dopamine in vivo with an enzyme based carbon fiber microbiosensor. *Analytical Chemistry, 82*(3), 989–996. https://doi.org/10.1021/ac9022605.
Novella-Rodríguez, S., Veciana-Nogués, M. T., Izquierdo-Pulido, M., & Vidal-Ca, M. C. (2003). Distribution of biogenic amines and polyamines in cheese. *Journal of Food Science, 68*(3), 750–755. https://doi.org/10.1111/j.1365-2621.2003.tb08236.x.
Nurul Karim, M., & Lee, H. J. (2013). Amperometric phenol biosensor based on covalent immobilization of tyrosinase on Au nanoparticle modified screen printed carbon electrodes. *Talanta, 116*, 991–996. https://doi.org/10.1016/j.talanta.2013.08.003.
Ordóñez, J. L., Troncoso, A. M., García-Parrilla, M. D. C., & Callejón, R. M. (2016). Recent trends in the determination of biogenic amines in fermented beverages – A review. *Analytica Chimica Acta*. https://doi.org/10.1016/j.aca.2016.07.045.
Petrova, J., Romanova, J., Madjarova, G., Ivanova, A., & Tadjer, A. (2012). Absorption spectra of model single chains of conducting polyaniline. *Journal of Physical Chemistry B, 116*(22), 6543–6552. https://doi.org/10.1021/jp301814u.
Shiraishi, Y., Tanaka, H., Sakamoto, H., Ichikawa, S., & Hirai, T. (2017). Photoreductive synthesis of monodispersed Au nanoparticles with citric acid as reductant and surface stabilizing reagent. *RSC Advances, 7*(11), 6187–6192. https://doi.org/10.1039/c6ra27771c.
Singh, S., Jain, D. V. S., & Singla, M. L. (2013). Sol-gel based composite of gold nanoparticles as matix for tyrosinase for amperometric catechol biosensor. *Sensors and Actuators, B: Chemical, 182*, 161–169. https://doi.org/10.1016/j.snb.2013.02.111.
Sujitha, M. V., & Kannan, S. (2013). Green synthesis of gold nanoparticles using Citrus fruits (*Citrus limon*, *Citrus reticulata* and *Citrus sinensis*) aqueous extract and its characterization. *Spectrochimica Acta - Part A: Molecular and Biomolecular Spectroscopy, 102*, 15–23. https://doi.org/10.1016/j.saa.2012.09.042.
Suresh, A. K., Pelletier, D. A., Wang, W., Broich, M. L., Moon, J. W., Gu, B., ... Doktycz, M. J. (2011). Biofabrication of discrete spherical gold nanoparticles using the metal-reducing bacterium *Shewanella oneidensis*. *Acta Biomaterialia, 7*(5), 2148–2152. https://doi.org/10.1016/j.actbio.2011.01.023.
Tan, Y., Kan, J., & Li, S. (2011). Amperometric biosensor for catechol using electrochemical template process. *Sensors and Actuators, B: Chemical, 152*(2), 285–291. https://doi.org/10.1016/j.snb.2010.12.021.
Telsnig, D., Kassarnig, V., Zapf, C., Leitinger, G., Kalcher, K., & Ortner, A. (2012). Characterization of an amperometric biosensor for the determination of biogenic amines in flow injection analysis. *International Journal of Electrochemical Science, 7*(11), 10476–10486.
Vicentini, F. C., Janegitz, B. C., Brett, C. M. A., & Fatibello-Filho, O. (2013). Tyrosinase biosensor based on a glassy carbon electrode modified with multi-walled carbon nanotubes and 1-butyl-3-methylimidazolium chloride within a dihexadecylphosphate film. *Sensors and Actuators, B: Chemical, 188*, 1101–1108. https://doi.org/10.1016/j.snb.2013.07.109.
Wang, B., Zheng, J., He, Y., & Sheng, Q. (2013). A sandwich-type phenolic biosensor based on tyrosinase embedding into single-wall carbon nanotubes and polyaniline nanocomposites. *Sensors and Actuators, B: Chemical, 186*, 417–422. https://doi.org/10.1016/j.snb.2013.06.016.
Yang, L., Xiong, H., Zhang, X., & Wang, S. (2012). A novel tyrosinase biosensor based on chitosan-carbon-coated nickel nanocomposite film. *Bioelectrochemistry, 84*, 44–48. https://doi.org/10.1016/j.bioelechem.2011.11.001.